International Journal of Scientific Research and Modern Technology (IJSRMT) ijsrmt.com
Volume 5, Issue 6, 2026
DOI: https://doi.org/10.38124/ijsrmt.v5i6.1520

Inorganic-Chemistry Approaches to the Treatment of Dye-Polluted Water: A Comparative Review of Five Methods

Hussein Abed Al-Hasan[1]

[1]Department of Chemistry, College of Science, University of Al-Qadisiyah, Al Diwaniyah, Diwaniyah,58001, Iraq

Publication Date: 2026/06/23

Abstract

Synthetic dyes are among the most visible and the most refractory of industrial water pollutants. With global production now exceeding 700,000 tonnes per year and 10–15% routinely lost to effluent streams, the textile, leather, paper and food industries together discharge coloured wastewaters whose toxicity, complexity and resistance to biodegradation make conventional treatment processes either ineffective or expensive. This review surveys five established treatment strategies through the lens of inorganic chemistry — the family of methods in which metal cations, metal-oxide semiconductors, transition-metal redox couples, coordination polymers and electroactive metal interfaces are the central actors. We examine, in turn: (i) adsorption on inorganic adsorbents (metal oxides, layered double hydroxides, zeolites, clays and mesoporous silicas); (ii) photocatalytic degradation on inorganic semiconductors (TiO_2, ZnO, $BiVO_4$, g-C_3N_4 and their heterojunctions); (iii) Fenton and Fenton-like advanced oxidation processes, including the more recent sulfate-radical AOPs centred on Co^{2+}, Cu^{2+} and Fe-based activation of peroxymonosulfate and peroxydisulfate; (iv) metal–organic frameworks and coordination polymers, in which the metal node is simultaneously the binding pocket and the catalytic centre; and (v) electrochemical methods, including electrocoagulation on Fe/Al sacrificial anodes, electro-Fenton and electrocatalytic oxidation on metal-oxide and boron-doped diamond anodes. For each method we summarise the underlying coordination and redox chemistry, the operational variables that govern performance, and representative literature data on dye removal efficiencies and mineralisation. The review closes with a comparative overview, the practical challenges of cost, sludge and stability, and the directions in which the inorganic-chemistry toolkit is likely to expand in the next decade.

➢ *Highlights*

- Five inorganic-chemistry families cover the physical, chemical and electrochemical removal of synthetic dyes.
- LDH and metal-oxide adsorbents reach Langmuir capacities of several hundred to >1500 mg g^{-1} for azo and basic dyes.
- TiO_2, ZnO, Bi-based oxides and g-C_3N_4 heterojunctions degrade 90–99% of model dyes under solar irradiation.
- Co^{2+}/Fe^{2+} activation of peroxymonosulfate gives complete decolorisation in minutes through $SO_4^{\bullet-}$.
- Fe/Al electrocoagulation and Fe-based MOF photo-Fenton are the most deployable inorganic technologies at present.

Keywords: *Dye Removal; Inorganic Chemistry; Metal Oxides; Layered Double Hydroxides; Photocatalysis; Fenton Chemistry; Sulfate-Radical AOPs; Metal–Organic Frameworks; Electrocoagulation; Water Treatment.*

I. INTRODUCTION

Synthetic dyes occupy a peculiar position among industrial water pollutants. The annual world production of dyestuffs now exceeds 700,000 tonnes, distributed across textile, paper, leather, plastics, food, cosmetics and pharmaceutical industries [1,2]. Of this, somewhere between 10 and 15% is routinely lost in dyeing-step effluents, producing coloured wastewater streams with concentrations of 10–10,000 mg L^{-1} that are both aesthetically intolerable and chemically resistant to conventional biological treatment. The textile sector alone has been estimated to be responsible for around 17–20% of all industrial water pollution worldwide. The synthetic

Al-Hasan , H. A. (2026). Inorganic-Chemistry Approaches to the Treatment of Dye-Polluted Water: A Comparative Review of Five Methods. *International Journal of Scientific Research and Modern Technology*, *5*(6), 127–138. https://doi.org/10.38124/ijsrmt.v5i6.1520

dyes used in modern industry azo, anthraquinone, triarylmethane, phthalocyanine, indigo and xanthene chromophores have been deliberately engineered for chemical and photochemical stability against light, washing, oxidation and microbial degradation, the very properties that subsequently complicate their removal from waste streams.

The treatment of dye-polluted water is therefore both a long-standing and persistently active problem, addressed by methods drawn from every part of the chemical sciences. The present review takes inorganic chemistry as the organising thread. We examine five distinct strategies in which inorganic species metal cations, metal-oxide semiconductors, transition-metal redox couples, metal nodes in coordination polymers, and electroactive metal interfaces are the central actors. For each method we describe the underlying coordination and redox chemistry, the operating variables that govern performance, and representative literature data on real dye systems. We then compare the five approaches side by side and identify the directions in which the inorganic-chemistry toolkit is most likely to expand. The aim is to provide a coherent overview of how the central concepts of inorganic chemistry Lewis's acidity, hard-soft acid-base selectivity, redox couples, band-gap chemistry and coordination geometry collectively underpin the treatment of one of the more visible categories of industrial water pollution.

II. SYNTHETIC DYES: CHEMISTRY AND THE WATER-POLLUTION CONTEXT

Synthetic dyes are most usefully classified by their chromophore the chemical structure that absorbs visible light and confers colour. Azo dyes, identified by one or more –N=N– linkages between aromatic rings, account for more than half of all colorants produced; methyl orange, Congo red, Reactive Black 5 and the Orange II family are representative examples. Anthraquinone dyes are the second largest class and dominate the blue-to-green shade range; phthalocyanines (Cu, Co or metal-free), indigo derivatives, triarylmethane cations and xanthene chromophores are commercially important in their own right [3,4]. A second, complementary classification is by ionic character: anionic (acid, reactive, direct), cationic (basic) and non-ionic (disperse) dyes interact with surfaces differently, and that distinction governs their behaviour toward charged adsorbents and the radicals they react with. Table 1 collects the principal classes.

The ecological case against discharging dyes to surface water has two components. The first is optical: even a few mg L^{-1} of a strongly absorbing dye reduces light penetration enough to suppress aquatic photosynthesis and disturb the autotrophic food web of receiving waters. The second is toxicological. Many azo dyes are not themselves acutely toxic, but they are reduced under anaerobic conditions in the gut, in soil or in sediment to aromatic amines whose carcinogenic potential is well established the benzidine-derived dyes were withdrawn from use precisely for that reason. Some metallised dyes additionally release the central metal (Cu, Cr, Co) into the environment on degradation, transferring the problem from one pollutant class to another.

Regulatory thresholds for colour and dye-related parameters are typically set on aggregate measures rather than on individual dye limits. The widely-adopted spectral absorption coefficient limits (SAK) for textile effluent discharged to municipal sewers are around 7, 5 and 3 m^{-1} at 436, 525 and 620 nm respectively; the European Union's Industrial Emissions Directive sets best-available-technique emission levels for total organic carbon, COD and colour in textile and tanning effluents; many national authorities additionally restrict total dissolved solids, COD, sulfate and residual metal content. The practical implication is unambiguous: any treatment process for compliance has to achieve decolorisation to within single-figure m^{-1} absorption coefficients while simultaneously meeting the broader COD and metal targets that accompany it.

Table 1 Major Synthetic Dye Classes — Chromophores, Ionic Character and Representative Examples.

Class	Chromophore	Ionic character	Representative dyes
Azo	One or more –N=N– linkages between aromatic rings	Anionic or cationic	Methyl orange, Congo red, Reactive Black 5, Orange II, Acid Black 194
Anthraquinone	9,10-Anthraquinone core	Anionic	Reactive Blue 19, Alizarin Red, Acid Blue 25
Triarylmethane	Triphenylmethyl cation	Cationic	Crystal violet, Malachite green, Methyl violet
Phthalocyanine	M-phthalocyanine (M = Cu, Co, Ni, metal-free)	Anionic / non-ionic	Reactive Blue 21, Direct Blue 86
Indigo / indigoid	2,2′-Biindolin-3,3′-dione	Non-ionic / anionic	Indigo, Indigo carmine
Xanthene	Xanthene oxygen-bridged tricyclic system	Cationic / anionic	Rhodamine B, Eosin Y, Fluorescein
Nitro / nitroso	Aromatic $–NO_2$ / –N=O	Anionic	Naphthol Yellow S, Acid Orange 3

III. FIVE INORGANIC-CHEMISTRY APPROACHES: AN OVERVIEW

Of the many treatment technologies described in the dye-effluent literature, five families are dominated by inorganic chemistry and account for the majority of the published performance data. The first is adsorption on inorganic adsorbents — metal oxides, layered double hydroxides, zeolites, clays and mesoporous silicas where the binding mechanisms (electrostatic attraction, anion exchange, surface complexation) are set by the surface chemistry of the inorganic phase. The second is photocatalytic degradation on inorganic semiconductors (TiO_2, ZnO, Bi-based oxides, g-C_3N_4), where band-gap excitation generates the reactive oxygen species that destroy the dye. The third is Fenton and Fenton-like advanced oxidation processes, organised around the redox cycling of transition-metal couples (Fe^{2+}/Fe^{3+}, Co^{2+}/Co^{3+}, Cu^{+}/Cu^{2+}) and including the more recent sulfate-radical AOPs that have substantially extended the operating pH window. The fourth is metal–organic frameworks and other coordination polymers, in which the metal node is simultaneously the binding pocket and the catalytic centre. The fifth is the electrochemical family electrocoagulation, electro-Fenton, electrocatalytic oxidation in which the inorganic chemistry is supplied at the electrode interface. Figure 1 maps the five methods on a single conceptual diagram, and Table 2 contrasts them on a single page.

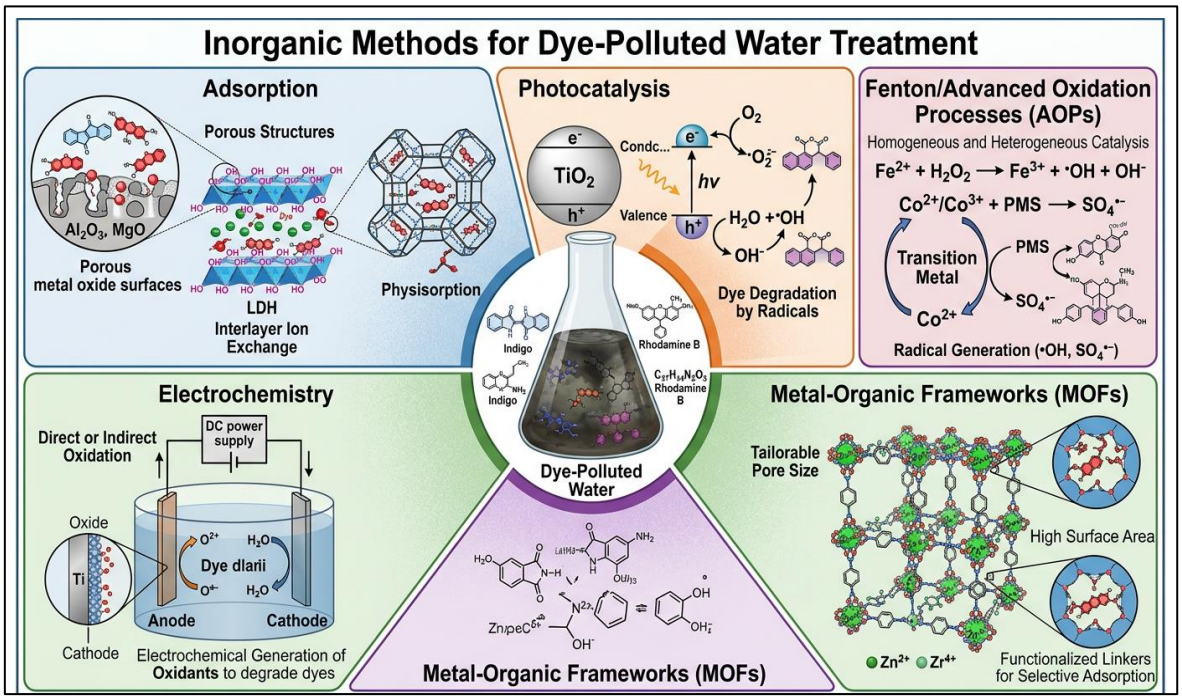

Fig 1 Conceptual Overview of the Five Inorganic-Chemistry Methods for Dye-Polluted Water Treatment Surveyed in this Review.

Table 2 Comparative Summary of the Five Inorganic-Chemistry Methods for Dye Removal.

Method	Active inorganic species	Mechanism	Typical efficiency	Main limitations
Adsorption on inorganic adsorbents	Metal oxides; LDH; zeolites; clays; mesoporous silica	Electrostatic; ion exchange; surface complexation; anion intercalation	70–>95% decolorisation; q up to ~1500 mg g^{-1}	Spent solid; regeneration; pH-sensitive
Photocatalysis on inorganic semiconductors	TiO_2, ZnO, $BiVO_4$, g-C_3N_4 and heterojunctions	Band-gap excitation → •OH and O_2•$^-$ ROS	90–99% degradation under UV-Vis	Catalyst recovery; photonic efficiency
Fenton and SR-AOPs	Fe^{2+}/Fe^{3+}; Co^{2+}/Co^{3+}; Cu^{2+}/Cu^{+} + H_2O_2 / PMS / PDS	Redox cycling → •OH or SO_4•$^-$ radicals	>95% decolorisation in minutes to 1 h	Iron sludge (classical); pH window
MOFs and coordination polymers	Fe^{3+}, Co^{2+}, Zr^{4+}, Cu^{2+} metal nodes with organic linkers	Adsorption + photo-Fenton + PMS activation on same scaffold	>90%, multi-cycle stable	Synthesis cost; hydrothermal stability
Electrochemical methods	Fe/Al sacrificial anodes; BDD, PbO_2, SnO_2 anodes; cathodic H_2O_2	Electrocoagulation; electro-Fenton; electrocatalytic •OH	87–98% decolorisation	Energy cost; electrode passivation

IV. METHOD 1: ADSORPTION ON INORGANIC ADSORBENTS

Adsorption is the most widely deployed dye-removal method on cost grounds, and the inorganic-adsorbent literature has expanded considerably over the last decade as researchers have looked for alternatives to activated carbon. Metal oxides Fe_3O_4, γ-Fe_2O_3, MnO_2, TiO_2, Al_2O_3 and ZnO combine moderate specific surface areas with reactive hydroxylated surfaces whose protonation/ deprotonation behaviour swings with solution pH; cationic dyes adsorb best on negatively charged oxide surfaces above the point of zero charge, while anionic dyes adsorb best below it [5,6]. Magnetite and maghemite add the practical advantage of magnetic recovery, allowing the loaded adsorbent to be lifted out of the treated water in a single step.

Layered double hydroxides (LDHs), often referred to as anionic clays, deserve a particular mention. They have the brucite-like layered structure $[M(II)_{1-x}M(III)_x(OH)_2]^{x+}\cdot[A^{n-}]_x/f\cdot mH_2O$, in which the divalent and trivalent cations (typically Mg^{2+}/Al^{3+}, Mg^{2+}/Fe^{3+}, Zn^{2+}/Al^{3+}, Ni^{2+}/Al^{3+}) carry a permanent positive layer charge balanced by interlayer anions. That positive layer charge is exactly suited to anion exchange against negatively charged sulfonate-bearing azo dyes such as Congo red, methyl orange and reactive dyes [7]. Calcined LDHs, in which the interlayer is collapsed to a mixed metal oxide, can additionally reconstruct the layered phase on contact with anionic solutions the so-called "memory effect" driving a remarkable adsorption capacity. Reported Langmuir capacities range from a few hundred mg g^{-1} on simple Mg–Al–CO_3 LDHs (487–559 mg g^{-1} for Orange I and Acid Red 114 on Mg–Al–5 00) up to >1000 mg g^{-1} on biocomposite-modified LDHs, with values as high as 1555 mg g^{-1} for methyl orange and 1112 mg g^{-1} for Congo red on starch-modified LDHs being among the highest in the literature [7,8].

Zeolites and clays offer a related family of inorganic adsorbents at very low cost. The aluminosilicate framework of zeolites (HY, ZSM-5, faujasites, mordenite) and the layered structure of clays (montmorillonite, kaolinite, bentonite, sepiolite) provide cation-exchange capacity that is particularly effective against cationic basic dyes; their surfaces can be modified by ion exchange with surfactants (organo-clays) to handle anionic dyes as well. Mesoporous silicas SBA-15 and MCM-41 bring ordered, narrow pore-size distributions and easily-functionalised silanol groups, and after grafting with amine, thiol or sulfonate functions they become selective adsorbents for specific dye classes. Representative capacities for inorganic adsorbents are gathered in Table 3.

The operating factors are the same as for any adsorption system. Solution pH is decisive and typically the variable optimised first, since it controls both the surface charge of the adsorbent and the ionisation state of the dye. Adsorbent dose, contact time, initial dye concentration, temperature and ionic strength complete the list. The equilibrium data are routinely interpreted with the Langmuir and Freundlich isotherms (Table 4) and the kinetics with pseudo-first-order, pseudo-second-order and intraparticle-diffusion models the same toolbox developed for heavy-metal adsorption. Inorganic adsorbents share the broader strength of the method (simple operation, low cost, often reusable through anion exchange or thermal regeneration) and the broader weakness (spent adsorbent becomes a secondary solid waste that itself requires disposal or regeneration).

Table 3 Representative Inorganic Adsorbents for Dyes — Composition, Target and Reported Langmuir Capacity (Values are Condition-Dependent and Indicative).

Adsorbent	Composition	Target dye	q_{max} (mg g^{-1})	Dominant mechanism
Mg–Al–CO_3 LDH	$Mg_6Al_2(OH)_{16}CO_3\cdot 4H_2O$	Acid Red 114	559	Anion exchange [7]
Mg–Al–5 00 (calcined LDH)	Mixed Mg–Al oxide	Orange I	487	Memory-effect reconstruction [7]
Starch-modified Mg–Al LDH	LDH/starch biocomposite	Methyl orange	~1555	Anion exchange + electrostatic [8]
Ni/Al LDH (starch-modified)	NiAl–CO_3 + starch	Congo red	329	Anion exchange [8]
Magnetite	Fe_3O_4 nanoparticles	Methylene blue	50–200	Electrostatic + magnetic recovery [5]
SBA-15 mesoporous silica	SiO_2 ordered mesopores	Methylene blue	~100–300	Silanol + pore filling [5,6]
Bentonite clay	Montmorillonite	Crystal violet	150–500	Cation exchange [6]
Zeolite (HY)	Aluminosilicate framework	Methylene blue	50–200	Cation exchange [6]

V. METHOD 2: PHOTOCATALYTIC DEGRADATION ON INORGANIC SEMICONDUCTORS

Heterogeneous photocatalysis is one of the most distinctive transformations that inorganic chemistry contributes to dye-effluent treatment, because in principle it allows complete mineralisation of the dye to CO_2, H_2O and small inorganic ions [9,10]. Anatase TiO_2 has been the prototype since Fujishima and Honda's 1972 demonstration of photoinduced water splitting at a TiO_2 electrode [11]. On illumination above the 3.2 eV band gap ($\lambda < 388$ nm), an electron is promoted to the conduction band and a hole is left in the valence band. Both species

react with surface-adsorbed water and oxygen to generate reactive oxygen species predominantly hydroxyl radicals (•OH, E° ≈ 2.80 V vs SHE) and superoxide anion radicals ($O_2^{\bullet-}$) which attack adsorbed dye molecules at the chromophore, initially cleaving the azo bond or hydroxylating the aromatic rings, and ultimately mineralising the carbon skeleton (Figure 2) [10,12].

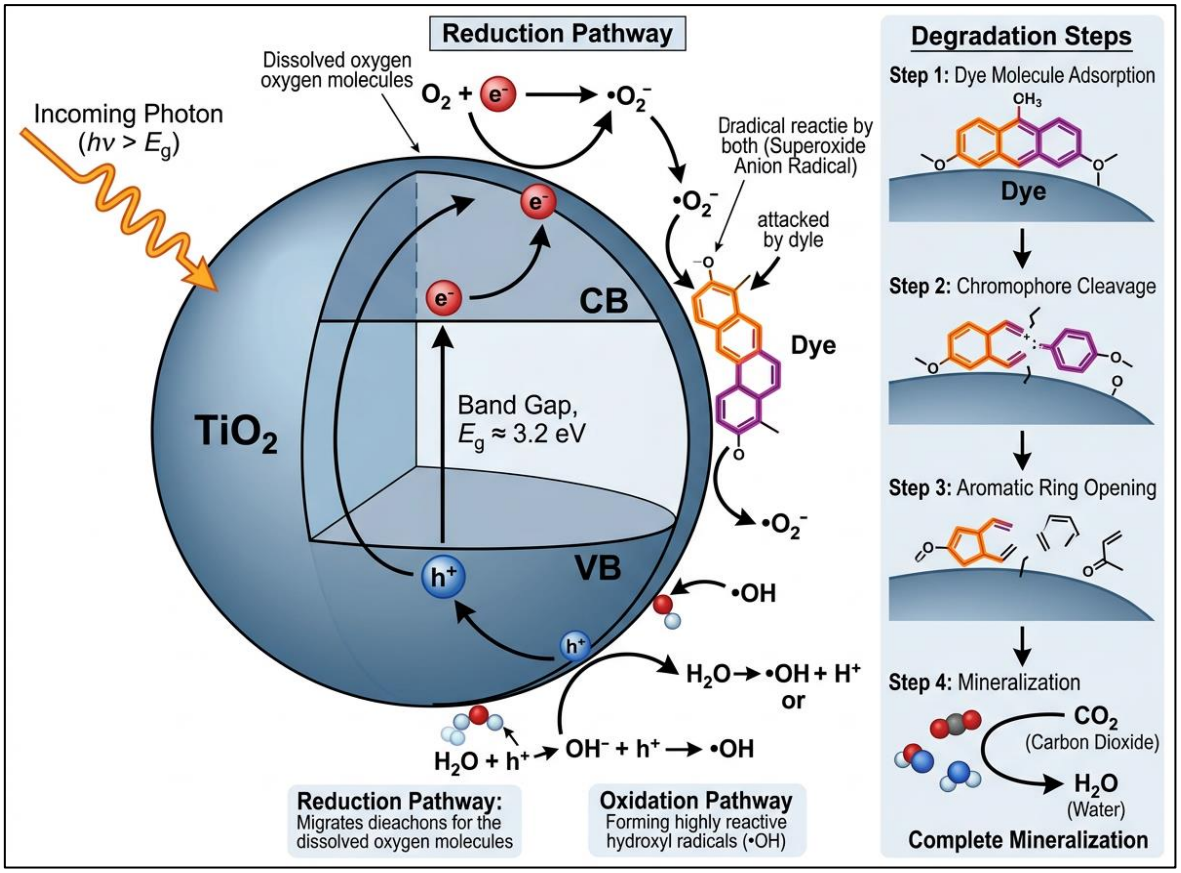

Fig 2 Illustration of the Photocatalytic Mechanism at a Semiconductor Nanoparticle Surface for Dye Degradation.

The chemistry has been extended in three directions, all of them firmly inorganic. The first is to broaden the response into the visible region, which contains the bulk of the solar spectrum. TiO_2 doped with metal cations (Fe^{3+}, Cr^{3+}, V^{4+}, Cu^{2+}) or with main-group anions (N^{3-}, S^{2-}, F^-) shows reduced effective band gaps; the same is true of carbon-modified TiO_2 in which incorporation of activated carbon lowers the effective gap to about 2.9 eV and increases visible-light response [12]. Composite catalysts have proved particularly effective: TiO_2/activated-carbon and TiO_2/reduced-graphene-oxide composites achieve 98.3% and 97% degradation of methylene blue respectively under solar irradiation in around 140 minutes, with substantial improvement in reusability over multiple cycles [12]. The second direction is to find semiconductors that absorb visible light intrinsically. ZnO (3.37 eV) plays a similar role to TiO_2 in the near-UV; $BiVO_4$, Bi_2WO_6, BiOCl and related bismuth-based oxides have band gaps of 2.4–2.8 eV that put their absorption edge into the visible, and the lone-pair-distorted Bi(III) coordination polyhedron typically results in well-separated photogenerated charges and high quantum efficiency [13]. The third direction is graphitic carbon nitride (g-C_3N_4), the metal-free polymeric semiconductor first introduced by Wang and colleagues in 2009 [14], with a ~2.7 eV band gap that places it in the visible region; it is now a standard visible-light photocatalyst for dye and pharmaceutical degradation.

The fourth, and increasingly dominant, family is the heterojunction. Two semiconductors with staggered band edges are placed in intimate contact so that the photogenerated electrons and holes are spatially separated across the interface — a Z-scheme or p–n junction structure that suppresses charge recombination and prolongs the carrier lifetimes that drive ROS generation. The Cu_2O/g-C_3N_4 Z-scheme heterojunction reported by Liu and co-workers achieves 98.3% degradation of methyl orange under visible light within 90 minutes and retains 93.7% of its initial activity even after 216 days of storage [15]. Analogous performance has been reported for TiO_2/g-C_3N_4, $BiVO_4$/g-C_3N_4, ZnO/TiO_2 and many other combinations. Representative photocatalytic degradation studies on common dyes are gathered in Table 5.

The operating variables of photocatalysis light intensity and wavelength, catalyst dose, dye initial concentration, dissolved oxygen and solution pH interact in complicated ways. Above an optimum catalyst dose, the suspension becomes opaque and the photonic efficiency drops; the same is true above an optimum dye concentration, at which the dye itself competes for the incident light. The practical challenges of catalyst recovery from small particle sizes, of efficient light delivery in turbid effluents, and of scaling to industrial flowrates, remain the main barriers between laboratory performance and full deployment.

Table 4 Common Isotherm and Kinetic Models Used to Analyse the Uptake of Dyes on Inorganic Adsorbents.

Model	Category	Underlying assumption	Information obtained
Langmuir	Isotherm	Monolayer adsorption on energetically uniform sites; saturating	Maximum capacity q_{max}; affinity; favourability (R_L)
Freundlich	Isotherm	Heterogeneous surface; empirical power law	Heterogeneity/intensity (n); relative capacity (K^f)
Temkin	Isotherm	Heat of adsorption decreases linearly with coverage	Adsorption-energy (heat) parameter
Dubinin–Radushkevich	Isotherm	Pore-filling on a heterogeneous surface	Mean free energy E (physisorption vs chemisorption)
Pseudo-first-order	Kinetic	Rate proportional to number of unoccupied sites	Rate constant k_1; physisorption-leaning uptake
Pseudo-second-order	Kinetic	Rate proportional to the square of unoccupied sites	Rate constant k_2 and q_e; often read as chemisorption
Intraparticle diffusion (Weber–Morris)	Kinetic	Uptake varies with $\sqrt{t}$ when pore diffusion controls	Diffusion rate; rate-limiting step
Elovich	Kinetic	Chemisorption on energetically heterogeneous surface	Initial sorption rate; desorption constant

Table 5 Representative Photocatalytic Degradation Studies of Dyes on Inorganic Semiconductors (Values are Condition-Dependent and Indicative).

Photocatalyst	Target dye	Light source	Efficiency	Time	Ref.
TiO_2 (anatase)	Methylene blue	UV / solar	93–98%	~140 min	[12]
TiO_2 / activated carbon	Methylene blue	Solar	98.3%	138 min	[12]
TiO_2 / reduced GO	Methylene blue	Solar	97%	~140 min	[12]
g-C_3N_4 (metal-free)	Rhodamine B; methyl orange	Visible	85–95%	60–180 min	[14]
Cu_2O / g-C_3N_4 (Z-scheme)	Methyl orange	Visible	98.3%	90 min	[15]
$BiVO_4$	Rhodamine B	Visible	80–90%	120 min	[13]
ZnO / Fe_3O_4 composite	Various dyes	UV-Vis	80–95%	60–120 min	[13]
g-C_3N_4 / TiO_2 heterojunction	Methylene blue	Visible	90–96%	90 min	[14]

VI. METHOD 3: FENTON AND FENTON-LIKE ADVANCED OXIDATION PROCESSES

If photocatalysis exemplifies one route to hydroxyl-radical generation, the Fenton reaction exemplifies the other. Discovered by H. J. H. Fenton in 1894, it has the elegantly simple stoichiometry $Fe^{2+} + H_2O_2 \rightarrow Fe^{3+} + {\bullet}OH + OH^-$ [16,17] and yields, at favourable conditions of pH 2.5–3.5, a strong oxidising radical (•OH, E° = 2.80 V vs SHE) capable of degrading essentially every organic dye into a sequence of smaller fragments and ultimately CO_2. The classical homogeneous Fenton process has been deployed at industrial scale for textile effluent for decades; it is operationally simple, fast and gives high colour removal, but it has three structural drawbacks. The pH window is narrow because Fe^{3+} precipitates as $Fe(OH)_3$ above pH 4, the Fe^{2+} to Fe^{3+} conversion is rapid but the back-reduction is slow so iron is consumed stoichiometrically, and the precipitated iron hydroxide constitutes a sludge that itself requires disposal.

Three modifications address these limitations. In the photo-Fenton process, near-UV–visible irradiation photoreduces $Fe(OH)^{2+}$ in solution to regenerate Fe^{2+} ($Fe(OH)^{2+} + h\nu \rightarrow Fe^{2+} + {\bullet}OH$), accelerating the catalytic cycle by an order of magnitude or more and yielding additional radicals. In electro-Fenton, hydrogen peroxide is generated in situ by two-electron oxygen reduction at a carbon-felt cathode ($O_2 + 2H^+ + 2e^- \rightarrow H_2O_2$) while Fe^{2+} is supplied either externally or by anodic dissolution of an iron electrode, eliminating the need to handle bulk H_2O_2. In heterogeneous Fenton, the iron is supported as an iron oxide (magnetite, hematite, goethite) or as a coordinatively-bonded Fe-MOF (MIL-53(Fe), MIL-100(Fe), MIL-101(Fe)), avoiding the iron-sludge problem and extending the working pH range upward to near-neutral [18,19]. MIL-100(Fe), with its ~2.7 eV band gap, has proved to be a particularly effective photo-Fenton catalyst: Fe_3O_4/MIL-100 composites and ZnO-decorated MIL-100 variants achieve more than 90% dye degradation under visible light over multiple cycles [19].

A more recent family has emerged around the activation of peroxymonosulfate (PMS, HSO_5^-) and peroxydisulfate (PDS, $S_2O_8^{2-}$) rather than hydrogen peroxide. The activated oxidants generate sulfate radicals ($SO_4{\bullet}^-$) whose standard reduction potential of 2.5–3.1 V is comparable to or slightly higher than that of •OH, and whose half-life of 30–40 µs is several orders of magnitude longer than the ~20 ns half-life of •OH [20,21]. Sulfate radicals therefore travel further before reacting, tolerate a wider pH range and show greater selectivity towards electron-rich aromatic substrates such as dye chromophores. Cobalt is the most effective non-noble

activator: $Co^{2+} + HSO_5^- \rightarrow Co^{3+} + SO_4^{\bullet-} + OH^-$. Heterogeneous cobalt-containing catalysts — Co-doped iron oxides, Co_3O_4, ZIF-67 and other Co-MOFs give complete decolorisation of model dyes such as Orange II, Rhodamine B and Congo red within minutes. A cobalt-doped mesoporous iron oxide reported by Suib and co-workers achieves complete degradation of Orange II within one minute under visible irradiation and operates stably over seven cycles with cobalt leaching as low as 0.5 ppm [22]; ZIF-67 catalyses PMS to fully decolorise high-concentration (100 mg L^{-1}) Rhodamine B within minutes across pH 3–9 [25]. Iron-based activation of PMS is operationally similar to Fenton chemistry but at lower H_2O_2 demand; copper, manganese and other transition-metal activators have also been reported. Table 6 collects representative examples. The Fenton family taken together has emerged as the dominant chemical-oxidation route for dye-effluent treatment, and the inorganic chemistry at its heart the controlled redox cycling of a transition-metal ion in the presence of an oxidant is the unifying theme of the entire family.

Table 6 Representative Fenton and Sulfate-Radical Advanced Oxidation Studies on Synthetic Dyes.

Catalyst / activator	Oxidant	Target dye	Efficiency	Conditions
Fe^{2+} (homogeneous Fenton)	H_2O_2	Methylene blue	>95% decolorisation	pH 3, 30 min [17]
UV / Fe^{2+} (photo-Fenton)	H_2O_2	Methyl orange	~99%	pH 3, 15 min [17]
Fe_3O_4 (heterogeneous Fenton)	H_2O_2	Rhodamine B	90–95%	pH 3–5, 60 min [18]
Co^{2+} (homogeneous)	PMS	Acid Black 194	99% decolorisation; 41% TOC removal	30 min / 240 min [21]
Co-doped mesoporous Fe oxide	PMS + visible light	Orange II	Complete	1 min; 7 cycles [22]
ZIF-67 (Co-MOF)	PMS	Rhodamine B (100 mg L^{-1})	Complete	Minutes; pH 3–9 [25]
Iron–cobalt bimetallic phosphide / Ni foam	PMS	Dye effluent	>95%	Minutes [21]
CUST-593 Co-MOF	PMS	Multiple dyes	>90%	Wide pH window [38]

VII. METHOD 4: METAL–ORGANIC FRAMEWORKS AND COORDINATION POLYMERS

Metal–organic frameworks (MOFs) and the broader family of coordination polymers occupy a special position in the inorganic-chemistry toolkit for dye treatment because they unite, on the same crystalline scaffold, the binding pocket and the catalytic centre. A MOF is built from a metal node a single ion or a cluster, typically Zn^{2+}, Cu^{2+}, Fe^{3+}, Zr^{4+}, Co^{2+}, Ni^{2+}, Al^{3+} coordinated through multidentate organic linkers (carboxylates, imidazolates, porphyrins, pyridines, sulfonates) into a porous, ordered network with specific surface areas routinely above 1000 $m^2\ g^{-1}$ and in some cases above 7000 $m^2\ g^{-1}$ [23,24]. The synthetic versatility is unusual: by choosing the node and the linker, one can tune pore size in the 0.5–5 nm range, vary the binding-site chemistry from soft (Cu, Zn) to hard (Zr, Al), incorporate photoactive linkers (porphyrins, naphthalenediimides), and post-synthetically functionalise pendant groups with task-specific ligands.

For dye removal, three classes of MOF have proved particularly useful. The iron-based MILs — MIL-53(Fe), MIL-100(Fe), MIL-101(Fe) combine high surface area with the redox-active Fe^{3+}/Fe^{2+} node, making them effective both as adsorbents and as heterogeneous photo-Fenton catalysts. MIL-100(Fe) has a band gap of ~2.7 eV that is well placed for visible-light photo-Fenton chemistry; composites with Fe_3O_4 or with ZnO push photo-Fenton dye-degradation efficiencies above 90% over multiple cycles. Fe_3O_4/MIL-100(Cr) achieves 92.4% Eosin Y degradation under visible light with >90% activity retained over three consecutive cycles [19]. Zr-based MOFs — UiO-66, UiO-67, MOF-808 combine exceptional chemical and hydrothermal stability with the Lewis-acidic Zr_6 node, suitable for adsorption of negatively charged sulfonate-bearing dyes; functionalisation with $–NH_2$, $–SO_3H$ or porphyrin units adds selectivity and visible-light response. Cobalt-, copper- and zinc-based MOFs such as ZIF-67, ZIF-8, HKUST-1 and the recently reported CUST-593 Co-MOF act as activators for PMS in sulfate-radical AOPs and have been shown to drive >90% decolorisation of Congo red and Rhodamine B within minutes [25,38]. Density functional theory calculations on ZIF-67 indicate HOMO–LUMO gaps below 0.02 eV for the relevant frontier orbitals, consistent with a low-barrier Co^{2+}/Co^{3+} redox cycle [25] a connection that draws directly on the molecular-orbital concepts familiar from molecular inorganic chemistry.

The synthetic chemistry of these materials draws directly on the same coordination concepts familiar from molecular chemistry: hard-soft acid–base matching of the metal node to the linker donor atoms; the ligand-field effects that determine the spin state and reactivity at the node; and the secondary building-unit (SBU) approach to topology design first articulated by Yaghi and co-workers. The catalytic chemistry on the node is also recognisably molecular: ligand-to-metal charge transfer (LMCT) populates the Fe(III) excited state at MIL-100(Fe) and drives the photocatalytic step, while open Co(II) sites in ZIF-67 act as Lewis acids that bind PMS and lower its activation barrier through inner-sphere electron transfer. The same scaffold can be designed to host an active species encapsulated noble-metal nanoparticles, immobilised enzymes such as horseradish peroxidase, or

embedded molecular catalysts converting it into a multifunctional bio-nanoreactor [26]. From the engineering side, the principal disadvantages of MOFs are the cost of synthesis at scale, the limited hydrothermal stability of many representatives, and the difficulty of recovering small crystallites from treated water challenges that are slowly being addressed through hollow-fibre and nanofibre membrane formats, magnetic compositing and on-surface synthesis (Figure 3). The trajectory, however, is clear: MOFs and coordination polymers are now one of the most actively investigated classes of inorganic material for dye treatment, and they sit at the intersection of three of the other methods reviewed here (adsorption, photocatalysis and Fenton chemistry).

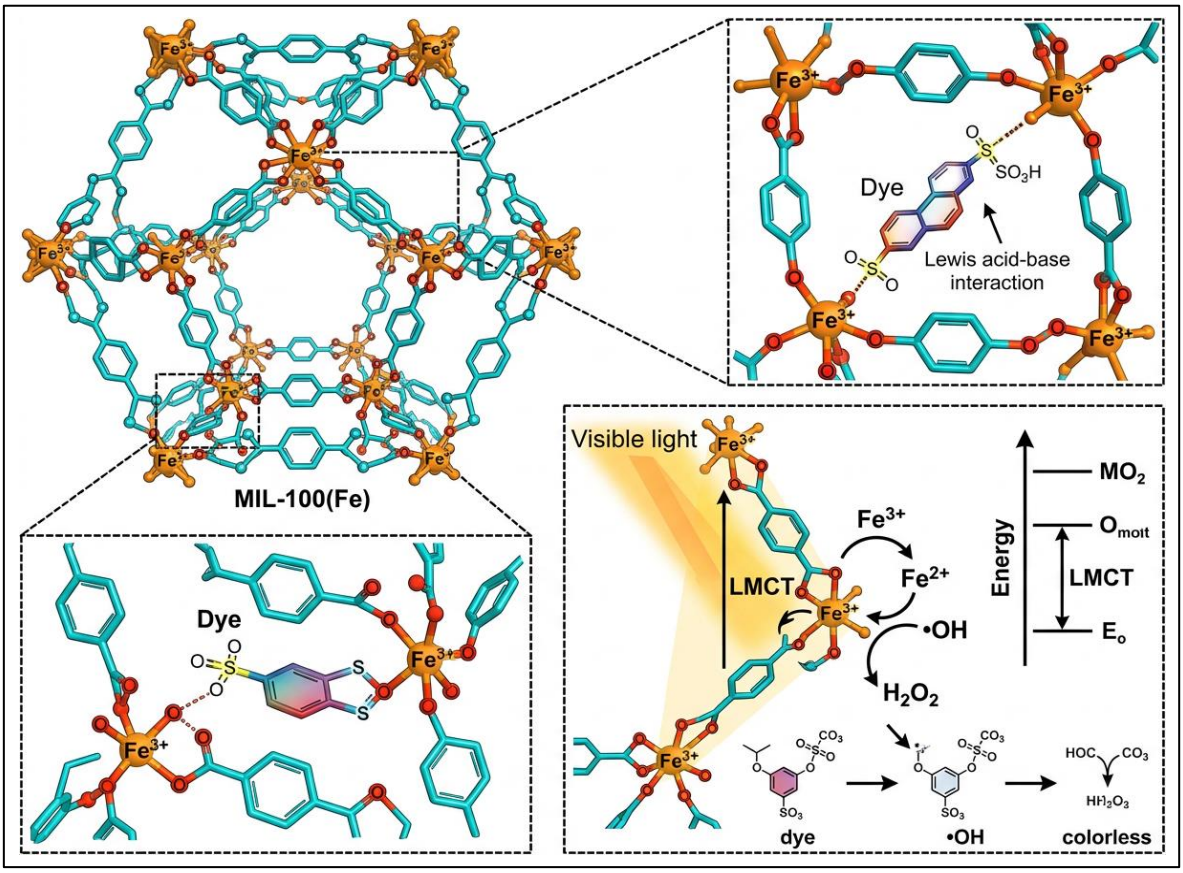

Fig 3 Illustration of Dye Binding and Photo-Fenton Catalysis at an Iron-Based MOF Metal Node.

VIII. METHOD 5: ELECTROCHEMICAL METHODS

Electrochemistry contributes the fifth major family of inorganic-chemistry routes for dye removal, in which the inorganic chemistry is supplied entirely at the electrode interface and the only added consumable, in principle, is electricity. Three sub-families dominate the literature.

In electrocoagulation, a sacrificial metallic anode almost always iron or aluminium is dissolved electrochemically ($Fe^0 \rightarrow Fe^{2+} + 2e^-$; $Al^0 \rightarrow Al^{3+} + 3e^-$). The metal cation released hydrolyses immediately through a sequence of charged hydroxo species and ultimately to amorphous $Fe(OH)_3$ or $Al(OH)_3$ colloids that bear extensive surfaces and adsorb dye molecules through electrostatic interaction, surface complexation and entrapment [27]. Simultaneous cathodic water reduction generates H_2 bubbles that flotation-lift the dye-loaded flocs to the surface. The process is operationally simple and works across a broad pH window. For real textile effluent, decolorisation efficiencies of 87–98% are routine on Fe or Al anodes at current densities of 0.5–4 mA cm^{-2} and contact times of 30–120 min, with typical energy demands of 1–5 kWh m^{-3} [27,28]. Comparisons of Fe and Al electrodes across various dye classes show Al gives marginally higher decolorisation for reactive and basic dyes (98% for Basic Yellow 28; 92% for Reactive Black 5 at 0.83 mA cm^{-2}) while Fe is generally preferred for disperse dyes and produces a denser, more easily separable sludge.

In electrocatalytic oxidation (also called electrochemical advanced oxidation), the dye is oxidised directly at the anode surface or, more usually, indirectly through •OH generated by oxidation of water on the anode ($M + H_2O \rightarrow M(\bullet OH) + H^+ + e^-$). The anode material is the critical choice. So-called "active" anodes (graphite, RuO_2, IrO_2) chemisorb the hydroxyl radical and oxidise only partially; "non-active" anodes boron-doped diamond (BDD), PbO_2, SnO_2–Sb generate weakly bound •OH and achieve full mineralisation of dye molecules at moderate current densities. BDD anodes in particular have become a small-scale standard for refractory effluents because of their wide potential window and chemical inertness [37].

In electro-Fenton, the two are combined: at the carbon-felt cathode, oxygen is electrochemically reduced to H_2O_2 in situ ($O_2 + 2H^+ + 2e^- \rightarrow H_2O_2$), and ferrous ion is added or generated by anodic dissolution to drive

classical Fenton chemistry, often coupled with anodic •OH generation at a BDD counter-electrode. The combination eliminates the need to transport and store H_2O_2 and gives the highest mineralisation efficiencies in the electrochemical family at the cost of additional energy consumption and electrode wear [37]. The principal limitations of the electrochemical methods are electrode passivation (particularly on Fe), the additional cost of electrical energy in regions where this is expensive, and concentrate management for the sludge or electrolyte streams. Their principal strengths modular scale, real-time process control, no external chemical addition beyond a supporting electrolyte make them increasingly attractive as the polishing step in hybrid treatment trains (Figure 4). Representative electrochemical and MOF dye-treatment studies are gathered in Table 7.

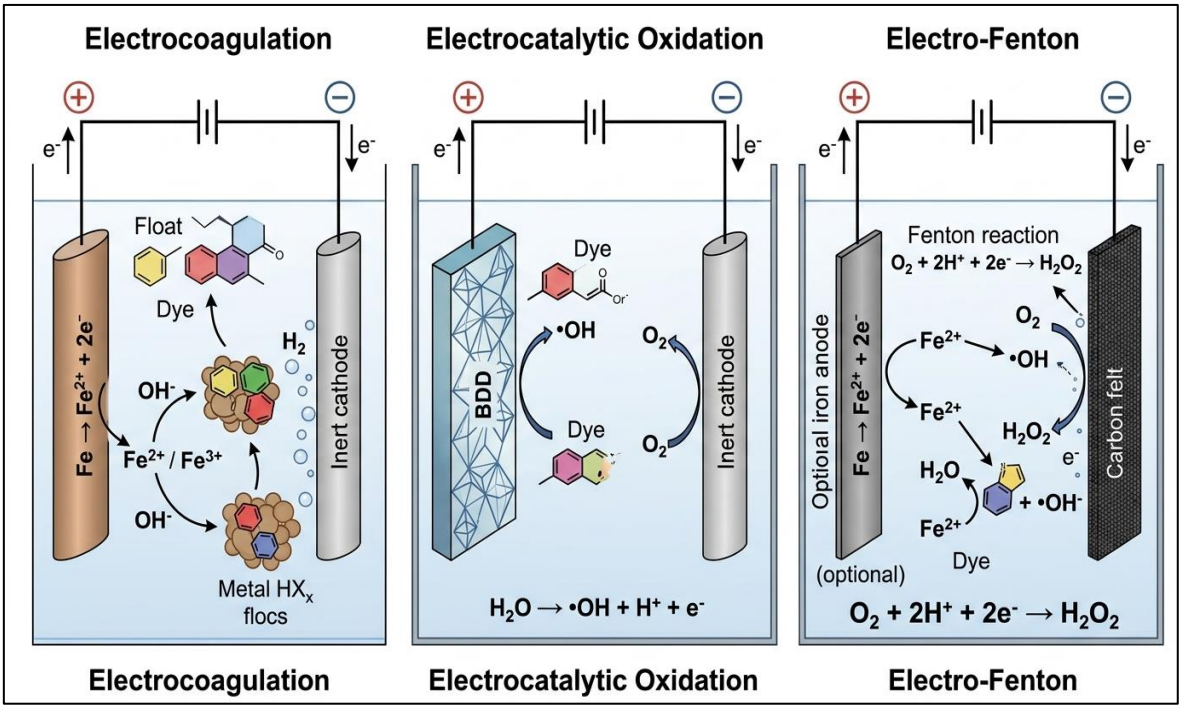

Fig 4 Illustration of Three Electrochemical Configurations for Dye Removal: Electrocoagulation, Electrocatalytic Oxidation on a BDD Anode, and Electro-Fenton.

Table 7 Representative MOF and Electrochemical Dye-Treatment Studies (Values are Condition-Dependent and Indicative).

System	Active inorganic chemistry	Target dye	Performance	Ref.
MIL-100(Fe)	Fe(III)/Fe(II) photo-Fenton; LMCT excitation	MB / MO / tetracycline	>90%, recycle-stable	[19]
Fe_3O_4 / MIL-100(Cr)	Composite photo-Fenton	Eosin Y	92.4%; >90% over 3 cycles	[19]
Cu_2O / g-C_3N_4 Z-scheme	p–n heterojunction	Methyl orange (+ SERS for 4-ATP)	98.3%; 93.7% activity after 216 d	[15]
ZIF-67 Co-MOF	Co^{2+}/Co^{3+} + PMS activation	Rhodamine B; Congo red	Complete in minutes	[25]
Fe sacrificial anode (EC)	Anodic Fe dissolution → $Fe(OH)_3$ flocs	Textile reactive effluent	87–98% (COD/colour)	[27,28]
Al sacrificial anode (EC)	Anodic Al dissolution → $Al(OH)_3$ flocs	Basic Yellow 28; Reactive Black 5	92–98%	[27]
BDD anode electro-oxidation	Weakly-bound •OH at diamond surface	Acid Orange 7; mixed effluent	>90% mineralisation	[37]
Carbon-felt / Fe^{2+} electro-Fenton	In-situ H_2O_2 + Fenton cycle	Dye effluent	>95% decolorisation	[37]

IX. COMPARATIVE OVERVIEW OF THE FIVE METHODS

The five families set out above operate on very different chemistry but address the same practical objective: the removal or destruction of synthetic dyes in water at concentrations from a few mg L^{-1} up to several g L^{-1}. Adsorption on inorganic adsorbents remains the lowest-cost option and the only one that can plausibly be deployed on agricultural and small-industrial scales; LDH and clay adsorbents in particular offer Langmuir capacities in the hundreds of mg g^{-1}, are easily regenerated through anion exchange or thermal recalcination, and produce a recoverable solid waste rather than a liquid one. Photocatalysis is the route that achieves the highest mineralisation under the gentlest conditions solar

irradiation plus dissolved oxygen but its practical deployment hinges on solving catalyst recovery and on the scaling of light delivery. Fenton and Fenton-like AOPs are the workhorse of industrial textile-effluent treatment plants today, particularly in their heterogeneous and electro-Fenton variants, and the rapid rise of sulfate-radical AOPs adds a useful alternative with a substantially wider pH window.

MOFs and coordination polymers occupy a research-driven role at present, but with the trajectory of cost reduction and the increasing maturity of formats suitable for continuous-flow operation, they are likely to become deployable within the next decade; their conceptual strength lies in unifying adsorption, photocatalysis and Fenton chemistry on a single scaffold. Electrochemical methods, particularly electrocoagulation, are already mature for medium-scale plants where electricity is cheap. The fact that all five families work, and work on overlapping but distinct ranges of dye class and concentration, means that in industrial practice they are usually combined: coagulation (or electrocoagulation) as primary treatment, biological treatment as polishing, and photocatalysis or Fenton chemistry for the refractory residue that the upstream stages cannot reach. The next generation of dye-treatment trains will probably combine two or more of these inorganic-chemistry approaches on a single platform.

X. CHALLENGES AND FUTURE PERSPECTIVES

Despite five decades of work, several practical issues continue to limit the deployment of inorganic-chemistry methods for dye treatment. Real textile effluents contain salt loads, surfactants, sizing agents and natural organic matter that compete for adsorbent sites and scavenge radicals; performance figures obtained on a single dye in deionised water rarely survive translation to a real effluent matrix without recalibration. Catalyst recovery from small particle sizes, and the prevention of secondary metal leaching from Fe-, Cu- and Co-based catalysts into the treated water, remain demanding outside structured-support formats. Cost is a barrier for MOFs and for BDD-anode electrochemistry at full scale; energy demand limits the deployment of electrocatalytic oxidation in regions with expensive electricity. The toxicity of degradation intermediates particularly the aromatic amines produced by anaerobic or reductive cleavage of azo dyes is well documented but routinely under-monitored in laboratory studies that report only decolorisation rather than mineralisation.

Several themes are likely to dominate the next decade. Solar-driven photocatalysts with truly visible-light response and low cost (g-C_3N_4, Bi-based oxides, Fe-MOFs) are an active frontier. Sulfate-radical AOPs are expanding rapidly because they extend the operating pH range of Fenton chemistry. Hybrid systems adsorbents that double as Fenton supports, photocatalysts that double as adsorbents, electrocoagulation followed by photocatalytic polishing are increasingly the norm. And the integration of in-situ monitoring through the nanomaterial-sensing approaches discussed in our companion reviews [29] is, in our view, the most likely route by which laboratory performance will translate into deployed technology.

XI. CONCLUSION

Inorganic chemistry supplies the central toolkit for the treatment of dye-polluted water. Metal oxides, layered double hydroxides, clays and mesoporous silicas drive adsorption; metal-oxide semiconductors and their heterojunctions drive photocatalytic degradation; transition-metal redox couples drive Fenton and sulfate-radical advanced oxidation processes; metal nodes in coordination polymers drive selective adsorption and multifunctional catalysis; and electrochemical interfaces drive electrocoagulation, electro-Fenton and electrocatalytic oxidation. The five methods are complementary rather than competing: each handles a different combination of dye class, concentration, matrix and budget, and the most effective modern treatment trains combine two or three of them on a single platform. The trajectory is unambiguous. As the cost of MOFs falls, as visible-light photocatalysts mature, as sulfate-radical AOPs replace classical Fenton in industrial deployment, and as electrochemical polishing becomes a standard final step, the inorganic-chemistry approach to dye-effluent treatment will increasingly converge on hybrid, multifunctional platforms organised around the central concepts of coordination chemistry, redox cycling and semiconductor physics.

REFERENCES

[1]. Crini G. Non-conventional low-cost adsorbents for dye removal: a review. Bioresour Technol. 2006;97(9):1061–1085.

[2]. Lellis B, Fávaro-Polonio CZ, Pamphile JA, Polonio JC. Effects of textile dyes on health and the environment and bioremediation potential of living organisms. Biotechnol Res Innov. 2019;3(2):275–290.

[3]. Hunger K, editor. Industrial Dyes: Chemistry, Properties, Applications. Weinheim: Wiley-VCH; 2003.

[4]. Zollinger H. Color Chemistry: Syntheses, Properties, and Applications of Organic Dyes and Pigments. 3rd ed. Zürich: Wiley-VCH; 2003.

[5]. Ali I, Asim M, Khan TA. Low-cost adsorbents for the removal of organic pollutants from wastewater. J Environ Manage. 2012;113:170–183.

[6]. Yagub MT, Sen TK, Afroze S, Ang HM. Dye and its removal from aqueous solution by adsorption: a review. Adv Colloid Interface Sci. 2014;209:172–184.

[7]. Mishra G, Dash B, Pandey S. Layered double hydroxides: a brief review from fundamentals to application as evolving biomaterials. Appl Clay Sci. 2018;153:172–186.

[8]. Adsorptive removal of dyes on starch-modified Mg–Al / Ni–Al LDH biocomposites — reported Langmuir capacities of 1555 mg g^{-1} (methyl

orange), 1112 mg g^{-1} (Congo red), 329 mg g^{-1} (Congo red) and ~559/487 mg g^{-1} (Acid Red 114, Orange I on Mg–Al–500). 2024–2025 [full bibliographic details to be verified].

[9]. Hoffmann MR, Martin ST, Choi W, Bahnemann DW. Environmental applications of semiconductor photocatalysis. Chem Rev. 1995;95(1):69–96.

[10]. Linsebigler AL, Lu G, Yates JT. Photocatalysis on TiO_2 surfaces: principles, mechanisms, and selected results. Chem Rev. 1995;95(3):735–758.

[11]. Fujishima A, Honda K. Electrochemical photolysis of water at a semiconductor electrode. Nature. 1972;238(5358):37–38.

[12]. Synergistic photocatalytic degradation of methylene blue using TiO_2 composites with activated carbon and reduced graphene oxide. Appl Water Sci. 2024 [full bibliographic details to be verified].

[13]. Tan HL, Amal R, Ng YH. Alternative strategies in improving the photocatalytic and photoelectrochemical activities of visible-light driven $BiVO_4$: a review. J Mater Chem A. 2017;5(32):16498–16521.

[14]. Wang X, Maeda K, Thomas A, et al. A metal-free polymeric photocatalyst for hydrogen production from water under visible light. Nat Mater. 2009;8(1):76–80.

[15]. Cu_2O/g-C_3N_4 dual-functional p–n heterojunctions: a high-performance SERS sensor and photocatalytic self-cleaning system. Nanoscale. 2024 [full bibliographic details to be verified].

[16]. Fenton HJH. LXXIII.—Oxidation of tartaric acid in presence of iron. J Chem Soc Trans. 1894;65:899–910.

[17]. Pignatello JJ, Oliveros E, MacKay A. Advanced oxidation processes for organic contaminant destruction based on the Fenton reaction and related chemistry. Crit Rev Environ Sci Technol. 2006;36(1):1–84.

[18]. Bokare AD, Choi W. Review of iron-free Fenton-like systems for activating H_2O_2 in advanced oxidation processes. J Hazard Mater. 2014;275:121–135.

[19]. Mesoporous MIL-100(Fe) decorated with ZnO nanosphere for photo-Fenton dye degradation; Fe_3O_4/MIL-100(Cr) for visible-light photo-Fenton degradation of Eosin Y (92.4%, 3 cycles). Appl Catal B Environ / Int J Environ Anal Chem. 2018–2025 [full bibliographic details to be verified].

[20]. Anipsitakis GP, Dionysiou DD. Radical generation by the interaction of transition metals with common oxidants. Environ Sci Technol. 2004;38(13):3705–3712.

[21]. Lee J, von Gunten U, Kim JH. Persulfate-based advanced oxidation: critical assessment of opportunities and roadblocks. Environ Sci Technol. 2020;54(6):3064–3081.

[22]. Cobalt-doped mesoporous iron oxide for visible-light photo-assisted PMS activation — complete Orange II degradation within 1 minute over 7 cycles. Appl Catal B Environ. 2019 [full bibliographic details to be verified].

[23]. Furukawa H, Cordova KE, O'Keeffe M, Yaghi OM. The chemistry and applications of metal–organic frameworks. Science. 2013;341(6149):1230444.

[24]. Wang C, Liu X, Demir NK, Chen JP, Li K. Applications of water-stable metal–organic frameworks. Chem Soc Rev. 2016;45(18):5107–5134.

[25]. Activation of peroxymonosulfate by ZIF-67 for sulfate-radical-based degradation of Rhodamine B and Congo red — complete degradation in minutes across pH 3–9; DFT analysis of the Co^{2+}/Co^{3+} redox cycle. RSC Adv / J Mol Struct. 2024–2025 [full bibliographic details to be verified].

[26]. Ran J et al. Rational design of MOF-based multifunctional bio-nanoreactor for chloramphenicol detection and photo-degradation. Adv Sci. 2025 [full bibliographic details to be verified].

[27]. Brillas E, Martínez-Huitle CA. Decontamination of wastewaters containing synthetic organic dyes by electrochemical methods: an updated review. Appl Catal B Environ. 2015;166–167:603–643.

[28]. Comparative electrocoagulation studies on textile dye effluent using iron and aluminium electrodes — 87–98% colour and COD removal at 30 V, pH 7, 30–120 min, 1–5 kWh m^{-3}; comparative Fe/Al decolorisation of Disperse Orange 30, Basic Yellow 28, Reactive Black 5, Vat Brown 1. J Hazard Mater / Int J Environ Sci Technol. 2010–2024 [full bibliographic details to be verified].

[29]. Companion review of this series: Advanced Nanomaterial Surfaces for the Detection and Removal of Organic and Microbial Pollutants in Water [internal reference].

[30]. Hummers WS, Offeman RE. Preparation of graphitic oxide. J Am Chem Soc. 1958;80(6):1339.

[31]. Stoller MD, Park S, Zhu Y, An J, Ruoff RS. Graphene-based ultracapacitors. Nano Lett. 2008;8(10):3498–3502.

[32]. Langmuir I. The adsorption of gases on plane surfaces of glass, mica and platinum. J Am Chem Soc. 1918;40(9):1361–1403.

[33]. Freundlich H. Über die Adsorption in Lösungen. Z Phys Chem. 1906;57:385–470.

[34]. Lagergren S. Zur Theorie der sogenannten Adsorption gelöster Stoffe. K Sven Vetenskapsakad Handl. 1898;24(4):1–39.

[35]. Ho YS, McKay G. Pseudo-second order model for sorption processes. Process Biochem. 1999;34(5):451–465.

[36]. Weber WJ, Morris JC. Kinetics of adsorption on carbon from solution. J Sanit Eng Div ASCE. 1963;89(2):31–60.

[37]. Brillas E, Sirés I, Oturan MA. Electro-Fenton process and related electrochemical technologies based on Fenton's reaction chemistry. Chem Rev. 2009;109(12):6570–6631.

[38]. Cobalt-MOF (CUST-593) activation of peroxymonosulfate for >90% dye degradation across a wide pH range. J Mol Struct. 2023–2024 [full bibliographic details to be verified].

[39]. Crini G, Lichtfouse E. Advantages and disadvantages of techniques used for wastewater treatment. Environ Chem Lett. 2019;17(1):145–155.
[40]. Robinson T, McMullan G, Marchant R, Nigam P. Remediation of dyes in textile effluent: a critical review on current treatment technologies. Bioresour Technol. 2001;77(3):247–255.
[41]. Schwarzenbach RP, Escher BI, Fenner K, Hofstetter TB, Johnson CA, von Gunten U, Wehrli B. The challenge of micropollutants in aquatic systems. Science. 2006;313(5790):1072–1077.